REVIEW ARTICLE
PUBLISHED ONLINE: 4 NOVEMBER 2015 | DOI: 10.1038/NNANO.2015.251
nature nanotechnology

Controlling upconversion nanocrystals for emerging applications

Bo Zhou[1], Bingyang Shi[2], Dayong Jin[2,3]* and Xiaogang Liu[1,4,5]*

Lanthanide-doped upconversion nanocrystals enable anti-Stokes emission with pump intensities several orders of magnitude lower than required by conventional nonlinear optical techniques. Their exceptional properties, namely large anti-Stokes shifts, sharp emission spectra and long excited-state lifetimes, have led to a diversity of applications. Here, we review upconversion nanocrystals from the perspective of fundamental concepts and examine the technical challenges in relation to emission colour tuning and luminescence enhancement. In particular, we highlight the advances in functionalization strategies that enable the broad utility of upconversion nanocrystals for multimodal imaging, cancer therapy, volumetric displays and photonics.

Photon upconversion is a nonlinear optical phenomenon known as an anti-Stokes emission in which the sequential absorption of two or more low-energy photons leads to high-energy luminescent emission[1–3]. This concept was first conceived as a theoretical possibility by the Dutch-American physicist Nicolaas Bloembergen in 1959[4]. His idea was to develop an infrared photon detector using superexcitation, to count infrared photons through their interaction with rare-earth or transition-metal ions embedded as impurities in crystalline materials, and to do this in such a way that infrared wave quanta would be principally counted through sequential absorptions in the successive excited levels of the given dopant ion. Although the prospect of achieving photon upconversion appeared promising, Bloembergen was unable to establish the validity of his idea because of a lack of coherent pumping sources. Nonetheless, for his pioneering work in the field of nonlinear optics, Bloembergen was recognized with a share of the Nobel Prize in Physics in 1981.

With the advent of lasers and their associated fibre-based technology, the quest to exploit upconverted optical signals from inorganic solids started in the mid-1960s in several groups. Notably, the landmark experiment to witness upconverted visible emission was reported in 1966 by François Auzel, and was based on energy transfer through the use of Yb^{3+} to sensitize Er^{3+} and Tm^{3+} (ref. 1). Such Yb^{3+}-sensitized upconversion was also observed by Ovsyankin and Feofilov independently in the same year[5]. Shortly afterwards, upconverted green emission was achieved from the Yb^{3+}–Ho^{3+} couple[6]. The field of photon upconversion has since inspired the design of near-infrared (NIR) upconverters to generate visible light suitable for many areas of application[1,2]. In the early days of development, laser and optical technological advances were a compelling application because upconversion lasing provides a simple alternative to nonlinear optical techniques for converting low energy laser stimulation into high-energy and long-lasting visible emissions[7].

Despite these important advances, the applications of upconversion materials in the biological and biomedical fields were still unclear in the early days of investigation[2]. One major challenge was to devise methods for making materials with tunable size and shape as well as desirable surface characteristics that are compatible with biological environments[8,9]. As surface quenching of luminescence by solvent molecules dominates in nanostructured phosphors[10,11], synthesis of nanophosphors through lanthanide doping with precisely controlled concentrations, compositions and emission profiles could become extremely difficult. As it happens, this problem has provided a strong motivation for the materials science community. Indeed, much of the recent resurgence of upconversion came from the widespread research on nanomaterials synthesis, in conjunction with the pressing demand for next-generation luminescent biomarkers[1,2,12–20].

In this Review, we focus on controlling photon upconversion in lanthanide-doped nanocrystals and particularly recent experimental progress in using these optical nanomaterials in many areas of investigation. We start with a brief introduction to the fundamental aspects of the upconversion phenomenon, followed by a discussion of the major limitations involving photon upconversion in nanostructured materials. Next we give a more detailed description of upcoming approaches that enable tailored emission colour and enhanced conversion efficiency. An important emphasis is placed on the integration of different functionalities for providing solutions in specific application domains, such as biological imaging, molecular detection, drug delivery and optoelectronics. The final section highlights key challenges, feasible improvements and perspectives for future developments.

Fundamental considerations

In contrast to commonly used organic fluorophores and quantum dots[2,21], upconversion nanocrystals are composed of an inorganic crystalline host matrix and trivalent lanthanide ions (Ln^{3+}) embedded in the host lattice (Fig. 1a). Early investigations on lanthanide-doped bulk materials enabled a profound comprehension of the underlying physics to be attained[1,22,23]. Unlike two-photon absorption and second-harmonic generation, photon upconversion features sequential, rather than simultaneous, absorption of incident photons. For efficient upconversion to proceed, physically existent intermediate states between the ground state and the emitting state are required to act as energy reservoirs. The lanthanides' $4f^n$ electronic configurations are split by appreciable electronic repulsion and spin–orbit coupling, leading to a rich energy-level pattern

[1]Institute of Materials Research and Engineering, A*STAR (Agency for Science, Technology and Research), 3 Research Link, 117602 Singapore, Singapore. [2]Advanced Cytometry Labs, ARC Centre of Excellence for Nanoscale BioPhotonics, Macquarie University, Sydney, New South Wales 2109, Australia. [3]Institute for Biomedical Materials and Devices, Faculty of Science, University of Technology Sydney, New South Wales 2007, Australia. [4]Department of Chemistry, National University of Singapore, 3 Science Drive 3, 117543 Singapore, Singapore. [5]Centre for Functional Materials, NUS (Suzhou) Research Institute, Suzhou, Jiangsu 215123, China. *e-mail: chmlx@nus.edu.sg; dayong.jin@uts.edu.au

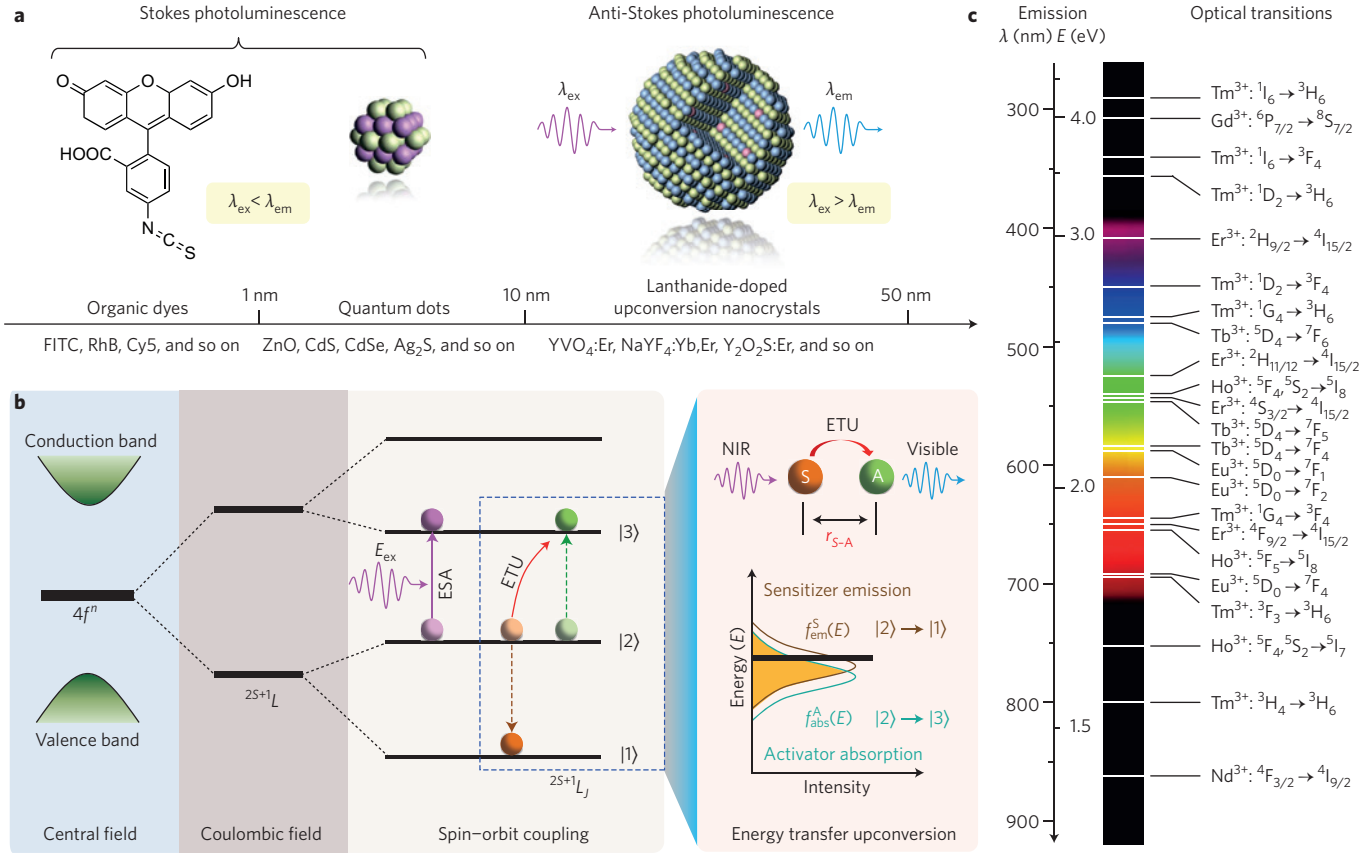

Figure 1 | Lanthanide-doped nanoparticles and photon upconversion. a, A comparison of three distinct classes of luminescent nanomaterials: organic dyes (left), semiconductor quantum dots (middle) and lanthanide-doped nanoparticles (right). In contrast to the two Stokes-type luminescent nanomaterials, upconversion nanoparticles feature an anti-Stokes emission with photon energy higher than the excitation source ($\lambda_{ex} > \lambda_{em}$). **b**, Electronic energy level diagrams of trivalent Ln^{3+} ions in relation to upconversion processes. The $4f^n$ electronic configuration splits into many energy sublevels due to the strong effects of the Coulombic interaction and spin–orbit coupling as well as weak crystal-field perturbation. The energy levels are represented by the symbol $^{2S+1}L_J$ (where S, L, J are the total spin, orbital and angular momentum quantum number of the electron, respectively), and optical transitions among these energy levels lead to abundant emission bands. In principle, a Ln^{3+} ion residing in an intermediate level $|2\rangle$ can be further promoted to an upper emitting level $|3\rangle$ through absorption of another photon E_{ex} (excited-state absorption (ESA) process), or through cooperative energy transfer between a pair of excited ions with one ion being non-radiatively decayed to the ground state $|1\rangle$ (energy transfer upconversion (ETU) process). The right inset panel shows that the realization of an efficient ETU process requires consideration of the sensitizer–activator distance (r_{S-A}), and the spectral overlap between sensitizer emission ($f^S_{em}(E)$) and activator absorption ($f^A_{abs}(E)$) profiles. **c**, Typical Ln^{3+}-based upconversion emission bands covering a broad range of wavelengths from ultraviolet (~290 nm) to NIR (~880 nm) and their corresponding main optical transitions.

(Fig. 1b). This attribute makes lanthanides ideal candidates for achieving photon upconversion. The lanthanides' $4f$ orbital electrons are partially filled and shielded by outer $5s$ and $5p$ electrons, giving rise to a weak electron–phonon coupling and hence sharp emission lines resulting from electronic transitions[24]. The photon upconversion also greatly benefits from a crystalline host lattice featuring a low phonon energy environment. For example, the non-radiative decay rate of lanthanides by multiphonon relaxation in such ionic crystals can be effectively suppressed. With the emergence of nanotechnology, upconversion emission can be precisely tuned to a particular wavelength spanning from the ultraviolet to the NIR region (Fig. 1c).

In principle, the upconversion mechanisms involving lanthanides can be mainly categorized into four classes[1,2]: excited-state absorption (ESA), energy transfer upconversion (ETU), cooperative sensitization upconversion (CSU) and photon avalanche (Box 1). It should be noted that the energy conversion is strongly dominated by the contributions of ETU. The ETU process typically occurs in a sensitizer–activator (S–A) system (Fig. 1b and Box 1). In such a system, the energy transfer from the sensitizer to the activator populates not only the emitting levels but also the intermediate levels, as evidenced in the case of Yb^{3+}–X^{3+} (X = Er, Tm or Ho) couples. According to Dexter's theory[25], the energy transfer probability W_{S-A} under a dipole–dipole interaction can be expressed by:

$$W_{S-A} = \frac{3h^4c^4}{64\pi^5 n^4 \tau_S} \times \frac{Q_{abs}}{r^6_{S-A}} \times \int \frac{f^S_{em}(E)\, f^A_{abs}(E)}{E^4} dE$$

where h, c, n, τ_S and r_{S-A} are Planck's constant, the speed of light in a vacuum, the refractive index, the intrinsic lifetime of the sensitizer and the S–A separation, respectively; Q_{abs} is the integrated absorption cross-section of the activator; $f^S_{em}(E)$ and $f^A_{abs}(E)$ are the normalized spectral line-shape functions of the emission band of the sensitizer at excited levels ($\int f^S_{em}(E)dE = 1$) and the absorption band of the activator at intermediate levels ($\int f^A_{abs}(E)dE = 1$), respectively. Therefore, we can derive that the S–A distance (r_{S-A}) and the spectral overlap (the integration term in the above equation) are the two critical parameters governing the energy transfer (Fig. 1b, right panel). Another criterion for achieving efficient energy transfer is the requirement of high absorbance (Q_{abs}) by the activator at the emission wavelength of the sensitizer. The Yb^{3+}–Er^{3+} couple is well suited to these requirements at 980 nm excitation.

Box 1 | Photon upconversion processes and dynamic analysis.

Photon upconversion of lanthanides (for example, Er^{3+}, Tm^{3+} and Ho^{3+}) is usually realized by either ETU or ESA, in which there are long-lived intermediate states to store the energy as shown below (panels **a** and **b**). In comparison, in the absence of such physically existent intermediate states (for example, Tb^{3+}) photon upconversion can be achieved by CSU (panel **c**)[140] or by energy migration (EM)-mediated upconversion within a core–shell structure[15] (panel **d**). Note that in the case of the energy migration approach, Tm^{3+} is generally employed as a ladder (L) to assist energy transfer (ET) from a sensitizer ion (S) to a migratory ion (M) and then an activator ion (A)[15]. Here, it should be pointed out that the extensively studied photon avalanche effect in bulk materials is seldom observed in upconversion nanocrystals. This might be due to the stringent conditions required for the establishment of an avalanche regime[141].

To probe the factor governing photon upconversion, we employ an ETU-based model as an example (panel **e**). In this model, it is assumed that all the activators residing in the emitting level contribute to the upconversion emission, and non-radiative decay processes in all excited states of both the sensitizer and activator ions are excluded. The populations of these states can be described by the following rate equations:

$$\frac{dn_5}{dt} = \Phi_P n_4 - \tau_5^{-1} n_5 - W_{ET} n_5 n_1 - W_{ETU} n_5 n_2$$

$$\frac{dn_2}{dt} = W_{ET} n_5 n_1 - \tau_2^{-1} n_2 - W_{ETU} n_5 n_2$$

$$\frac{dn_3}{dt} = W_{ETU} n_5 n_2 - \tau_3^{-1} n_3$$

where n_i (i = 1–5) denotes the population of ions at five different energy levels, τ_j (j = 2,3,5) denotes the lifetime of the excited energy level, and Φ_P, W_{ET}, W_{ETU} represent the effective pump rate and the coefficients of ET (labelled with 1) and ETU (labelled with 2) processes, respectively. Under a steady-state condition, the quantum yield (QY), defined as the ratio of the number of photons emitted to that of photons absorbed, can be obtained by the following relation:

$$QY = \frac{A_3 n_3}{\Phi_P n_4} = \frac{1}{2}\left[1 - \frac{1}{\Phi_P}\left(\frac{1}{\tau_2}\frac{n_2}{n_4} + \frac{1}{\tau_5}\frac{n_5}{n_4}\right)\right]$$

where A_3 is the spontaneous transition rate of the activator from the emitting level to the ground state. Hence, a high quantum yield requires a large effective pump rate and low populations of the sensitizer and activator in the excited state and intermediate state, respectively. The quantum yield can also be improved by using an activator with a long-lifetime intermediate state. From the equation for QY above, one can find that the limit of quantum yield for an ideal two-photon upconversion is close to 50%. However, the values of quantum yield measured through the use of an integrating sphere are typically low, for example, 0.1% for 30 nm $NaYF_4$:Yb,Er particles[42], indicating that the surface quenching effect dominates in small-sized nanoparticles.

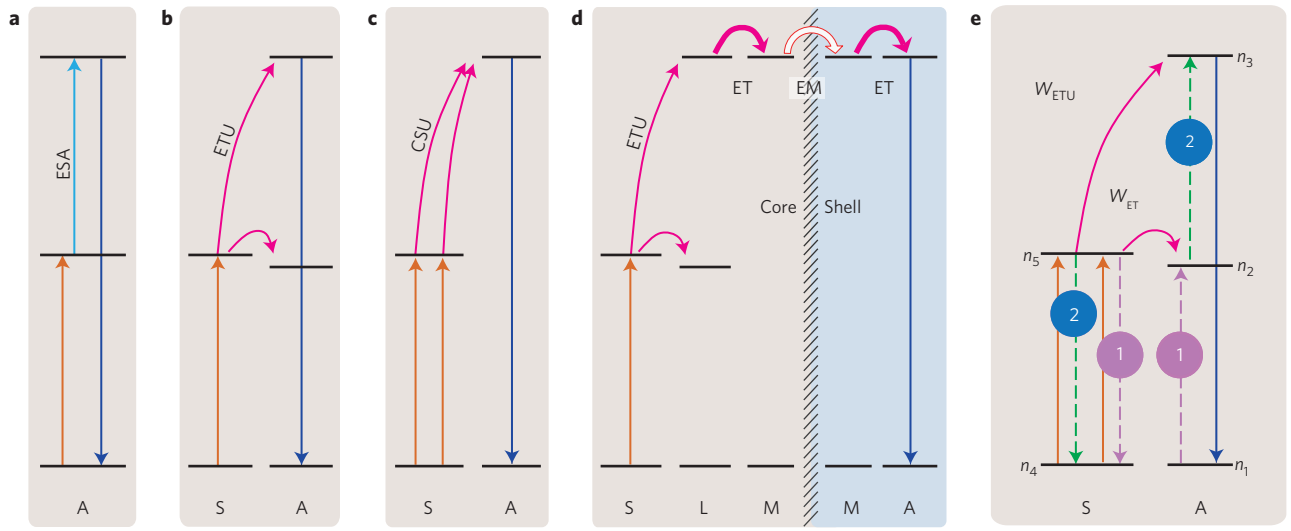

If there was an energy mismatch, W_{S-A} would decrease exponentially, depending on the magnitude of the mismatch. However, it could be partially compensated by the participation of matrix phonons, which can bridge the energy gap if it is not too large, as is the case with Yb^{3+}–Tm^{3+} and Yb^{3+}–Ho^{3+} couples. This process is termed phonon-assisted energy transfer.

Using the well-established rate equation model (Box 1) for lanthanide-doped bulk materials and devices[1], photon upconversion and its dynamic process in nanocrystals can be quantitatively predicted[19]. The microscopic parameters in the rate equation model can be approximately determined by Judd–Ofelt theory[26,27]. Importantly, recent developments in computational methods have permitted robust design of complex materials systems and accurate prediction of new properties by including subtle electronic perturbations in the physical characteristics of these materials[28–30]. For example, a kinetic model for elucidating the mechanism underlying spectrally pure emission has been developed by taking into account all possible absorption and radiative or non-radiative energy transfer[28]. With magnetic dipole transitions factored in, a detailed free-ion Hamiltonian can be used to quantify the magnetic component of light emission in trivalent lanthanides[30]. Combining these quantum-mechanical calculations with experimental results allows

the understanding of upconversion mechanisms involving 4*f* orbital electrons in a much greater level of detail than in the past.

To obtain high-quality upconversion nanocrystals, many efforts have been devoted to developing facile synthetic methods[21], such as co-precipitation[31], thermal decomposition[10], hydro(solvo)thermal synthesis[32], sol–gel[33] and microwave-assisted synthesis[34]. As a result, a wealth of compounds ranging from oxides (for example, Y_2O_3, ZnO and $Yb_3Al_5O_{12}$)[35–37] to fluorides (for example, CaF_2, $NaYF_4$ and $KMnF_3$)[31,38–40] have been synthesized and studied as host materials, among which hexagonal-phase $NaYF_4$ was acknowledged to be one of the most efficient upconversion hosts[41]. The availability of these versatile, readily scalable methods builds up the solid foundation necessary to implement the commercialization of upconversion nanomaterials.

Controlling photon upconversion

The upconversion emission of lanthanide-doped nanocrystals can be precisely controlled, in terms of emission colour, lifetime and intensity, for both advanced research and diverse practical applications.

Upconversion luminescence enhancement. Photon upconversion is an anti-Stokes-type emission, which is generally more complex than a Stokes-type emission. In a typical S–A-coupled nanocrystal system, the upconversion process is primarily governed by the following conditions: (1) the sensitizer's absorption capacity on excitation energy; (2) energy transfer efficiency from the sensitizer to the activator; (3) the radiative transition probability of the activator from the emitting state to a specific energy state; and (4) luminescence quenching effects.

For a nanoparticle with a large amount of activators doped at the surface, quenching of upconversion luminescence is inevitable, leading to an upconversion efficiency that is much smaller than that using its bulk counterpart[11,42]. An effective solution is to grow epitaxial shell layers by which the surface quenching effect can be largely minimized[10,11,38,43]. Such surface-protection strategies have been extensively applied to heterogeneous core–shell structures such as $NaYF_4$@$NaGdF_4$, $NaYF_4$@CaF_2 and CaF_2@$NaYF_4$ (refs 32,44,45). In this approach, the epitaxial growth of high-quality shell layers with less defective sites at the interface of the core–shell region is of critical importance[43,44,46].

Another interesting approach to enhancing photon upconversion is harnessing the effect of surface plasmon resonance (SPR). Noble metal nanoparticles such as gold and silver are frequently utilized. Note that the size and shape of the metal nanoparticles, as well as their distance to the luminescent centre are vital factors in regulating the band intensity and wavelength of SPR[47,48]. Thus, many schemes have been explored to tune and optimize the interaction between the metal and upconversion nanoparticles. These include the coating of a metal shell on the surface of upconversion nanoparticles[49], a double-shell coating comprising an intermediate SiO_2 layer and an outer metal layer[50], the coupling of Au nanoparticles to upconversion nanoparticles[48], the multilayer fabrication of close-packed upconversion and metal nanoparticles[51], and the construction of 3D plasmonic nanoantennas[52].

Recent experimental investigations suggest that upconversion luminescence can be enhanced by manipulating the local crystal field around the activators by codoping Li^+ or Sc^{3+} into a lanthanide-based nanocrystal[40,53]. The large size mismatch between the dopant and the host is likely to cause local distortion in the crystal lattice, allowing the site symmetry of the activators to be reduced. Consequently, this may lead to an increase in the probability of intra-4*f* optical transitions. Other notable strategies include broadband or super-high power excitation[54,55], energy clustering at the sublattice[56] and sensitization amplification through the use of synthetic infrared dyes[16,57]. The Yb^{3+}–MoO_4^{2-} dimer[37] or a metal-coated cantilever[58] have been proposed and experimentally validated for enhanced upconversion emission. However, it is noteworthy that their underlying mechanisms remain debatable, and claims of improved efficiency need to be verified and held to a robust standard[59,60]. It remains to be seen what further applications will benefit from the enhancement of upconversion luminescence.

Photon upconversion tuning. For applications in full-colour displays and multiplexed encoding, precise control over the emission profiles of upconversion nanocrystals in the form of emission colour and lifetime is required. The core–shell strategy, frequently used for nanoparticles with enhanced emission intensity, can also be adopted to allow fine tuning of the emission colour[61]. One difficulty with this is the stringent control of the shell thickness that is required to produce a colour of high chromatic purity. Alternatively, controlling dopant composition[31] and concentration[17], power density[55], host lattice[62] and excitation wavelength[63] of the nanocrystals provides convenient solutions tailored to their respective emission requirements. In view of the lanthanides' ladder-like electronic energy structure, control of energy transfer by means of selective doping can be used to modulate the energy population process and thus the emission colour. For instance, the incorporation of Ce^{3+} into Ho^{3+}-doped host lattices, either in nanoparticle or bulk form, leads to a marked change in emission colour from green to red. On a separate note, fine tuning of upconversion emission can be achieved using activators without long-lived intermediary energy states through energy-migration-mediated upconversion in core–shell structures[15]. This study was inspired by the ability of a gadolinium sublattice to mediate energy exchange over long-distance migration[15].

Exploiting new frontiers and applications

Over the past decade, research on upconversion nanocrystals has made tremendous progress, particularly in the realm of bioapplications, such as imaging, sensing and cancer therapy, because of their outstanding merits, such as multicolour emission capability under single-wavelength excitation, high signal-to-noise ratio, low cytotoxicity, and high chemical- and photo-stability[64–71]. As there are a number of related reviews already published regarding the application of upconversion nanocrystals in the area of bioapplications[21], herein we plan to focus on key developments of new properties and exploitation of these properties for emerging applications.

In 2009, non-blinking and photostable upconversion luminescence was first demonstrated on a single $NaYF_4$:Yb,Er nanoparticle (Fig. 2a)[72]. A similar design involving a series of ultrasmall $NaYF_4$:Yb,Er nanoparticles was later conceived to realize single-molecule tracking and imaging[73]. In 2010, a rewritable optical storage system with nondestructive readout was developed by Yan and co-workers[14], built on upconversion luminescence modulation of ordered nanopatterns comprising $NaYF_4$:Yb,Er nanoparticles (Fig. 2b). By making use of lanthanide-doped photocatalytic nanomaterials (for example, TiO_2:Er) or combining upconversion nanocrystals with plasmonic and semiconductor nanomaterials, NIR light photocatalysis has been demonstrated by a handful of research groups[74–76]. Another notable development was the fabrication of a NIR-light-responsive transistor by sandwiching a composite layer, consisting of 3D photonic crystals and $NaYF_4$:Yb,Tm nanoparticles, between a glass substrate and carbon nanotube thin films[77]. The NIR light sensitivity was about ten times higher than the control obtained with carbon nanotubes alone.

Recently, photon upconversion techniques have allowed researchers to implement fibre-optic sensing with ultrahigh sensitivities. For example, Jin and co-workers demonstrated remote sensing of a single nanoparticle travelling inside a microstructure optical fibre, with three orders of magnitude improvement over the sensitivity achieved by quantum dot-based techniques[56]. By deploying Er^{3+}-doped nanoparticles in optical devices, upconversion lasing and infrared signal

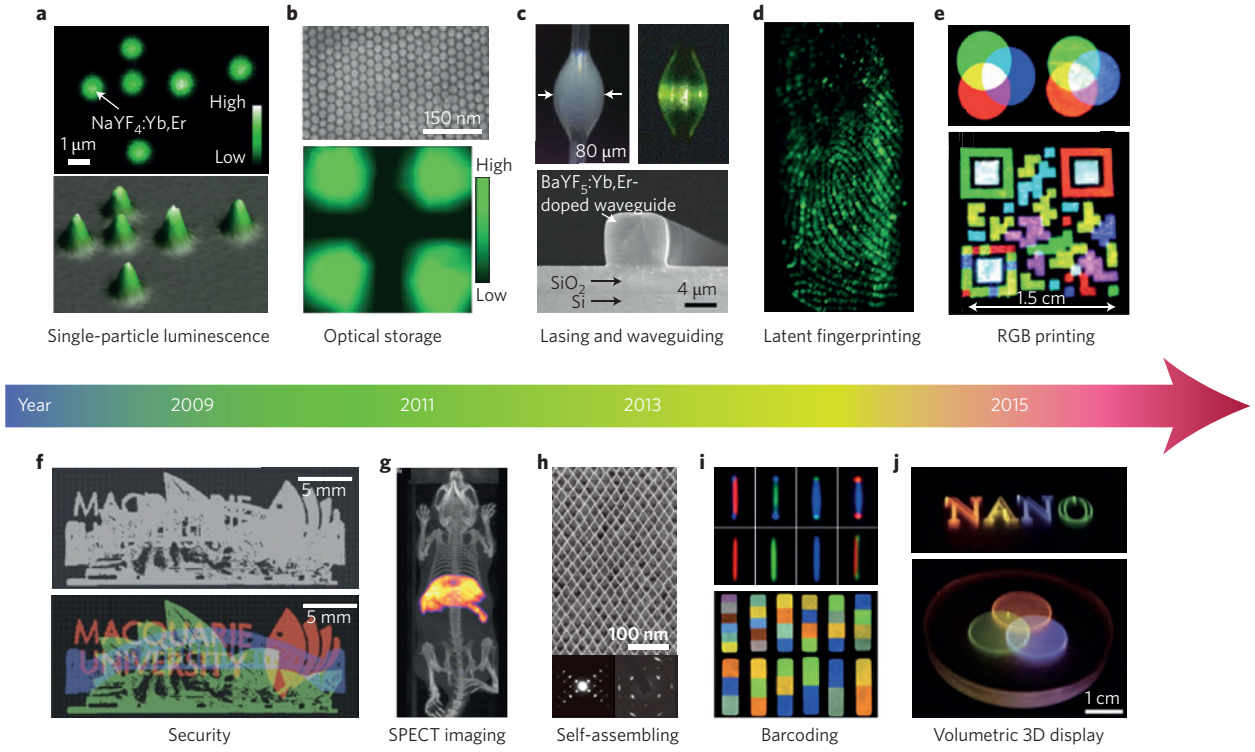

Figure 2 | Selective milestones in multifunctionalization of upconversion nanoparticles for emerging applications. a, Confocal imaging of $NaYF_4$:Yb,Er nanoparticles at the single-particle level. The colour scale represents photon counts. **b**, Rewritable optical storage enabled by patterned NIR-light-responsive nanoparticles. Scanning electron microscope image (top) and luminescence mapping image (bottom) of patterned substrates consisting of $NaYF_4$:Yb,Er nanoparticles. The colour scale represents the photoluminescence intensity. **c**, Lasing and waveguide amplifier using the nanoparticles as gain media. Top: Photographs of the $NaYF_4$:Yb,Er@$NaYF_4$-containing microcavity before (left) and after (right) pulsed laser excitation at 980 nm. Bottom: Scanning electron microscope image of the waveguide device modified with $BaYF_5$:Yb,Er@$BaYF_5$ nanoparticles. **d**, Latent fingerprinting through the use of $NaYF_4$:Yb,Er nanoparticles. **e**, Red–green–blue (RGB) printing involving nanoparticle inks. Top: Schematic design for creating secondary colours (left) and the corresponding image of the experimental result (right). Bottom: Multicolour barcode printing using $NaYF_4$:Yb,Er(Tm) nanoparticles. **f**, Demonstration of document security printing, made possible by three sets of lifetime encoded $NaYF_4$:Yb,Tm nanoparticles. The overlaid patterns (top) printed with nanocrystals having three distinct lifetimes can be decoded (bottom) by a time-resolved confocal fluorescence microscope equipped with a 980 nm laser. **g**, *In vivo* whole-body 3D imaging involving single-photon emission computed tomography (SPECT) through the use of ^{153}Sm-radioactivated $NaLuF_4$:Yb,Tm nanoparticles. **h**, Self-assembly of fluoride-based nanoplates. Top: Electron microscope image of a 2D superlattice of DyF_3 rhombohedral nanoplates. Bottom: Small-angle (left) and wide-angle (right) electron diffraction patterns of the superlattice. **i**, Multicolour barcoding through single particles. Top: Optical micrograph of dual-colour-banded single-crystalline microrods. Bottom: Luminescence image of multicolour-banded rod-shaped particles fabricated by microfluidic devices. **j**, Full-colour volumetric 3D display using pulse-duration-sensitive nanoparticles. Figure reproduced with permission from: **a**, ref. 72, NAS; **b**, ref. 14, Wiley; **c** (top), ref. 78, American Chemical Society; **c** (bottom), ref. 39, RSC; **d**, ref. 79, Wiley; **e**, ref. 80, RSC; **f**, ref. 17, Nature Publishing Group; **g**, ref. 94, Elsevier; **h**, ref. 96, Nature Publishing Group; **i** (top), ref. 97, American Chemical Society; **i** (bottom), ref. 98, Nature Publishing Group; **j**, ref. 19, Nature Publishing Group.

amplification could be achieved (Fig. 2c)[78,39], making upconversion nanomaterials suitable as optical gain medium in optoelectronics. Important advances in utilizing upconversion nanoparticles as inks for security applications, such as latent fingerprinting (Fig. 2d) and quick response code printing (Fig. 2e), have also been demonstrated[79,80]. Shining a beam of NIR light over the printed area converts the covert inks into a visible pattern. This printing scheme adds another level of security, providing an innovative means for data protection and identification.

It is well established that lanthanide-doped nanoparticles can support down-conversion emissions over broad spectral ranges, for example, the blue-to-infrared emission through the Pr^{3+}–Yb^{3+} couple[81]. Strategies of combining both up- and down-conversion hold promise for improving the conversion efficiency of existing photovoltaic installations by maximizing the use of sunlight in the infrared and ultraviolet–visible spectral region[82–87]. Apart from spectral fingerprints, the different lifetime decay rates (from μs to ms) of upconversion nanocrystals under a single-wavelength excitation can be utilized as a new dimension for multiplexing in the time domain — a rarely explored parameter readily extendable to the development of anti-counterfeiting measures, security and data storage technology[17,88–90] (Fig. 2f).

Meanwhile, developing new functions necessitates the utilization of the unique properties of Ln^{3+} ions. As an example, the green emission of Er^{3+} shows a highly sensitive spectral response in the form of peak intensity ratio or emission wavelength to temperature and pressure, suggesting the potential use of Er^{3+}-doped nanoparticles for applications such as ultrasensitive thermometers or pressure sensors[36,91,92]. Furthermore, the ability to precisely tune upconversion emission in Ln^{3+}-doped $NaGdF_4$ nanoparticles through external magnetic manipulation offers new opportunities for the detection of magnetic fields with sensitivity comparable to conventional magnetometers of equivalent spatial resolution[93]. By introducing a small amount of radioactive ^{153}Sm into $NaYF_4$:Yb,Tm nanoparticles, single-photon emission computed tomography (SPECT) imaging is achievable[94], allowing for optical and SPECT dual-modal imaging (Fig. 2g). The high X-ray absorption coefficient of lutetium makes $NaLuF_4$ a promising candidate as a contrast

agent in X-ray computed tomography (CT) imaging[95]. By controlling the shape of nanocrystals and their interactions, formation of nanocrystal superlattices has been successfully realized (Fig. 2h)[96].

Through control over the crystal growth by hydrothermal synthesis, Zhang *et al.*[97] prepared a series of single-crystalline microrods that can emit different colour patterns by varying precursor composition from the centre to the ends (Fig. 2i, top). In contrast, Doyle and co-workers[98] fabricated a unique encoding architecture by micropatterning spectrally distinct upconversion nanocrystals and demonstrated large, exponentially scalable encoding capacities (>10^6 particles) with an ultralow decoding false-alarm rate (<10^{-9}) (Fig. 2i, bottom). The design flexibility afforded by micropatterning allows for the possibility of optical barcoding for applications in anti-counterfeiting and multiplexed labelling. Most recently, Deng *et al.*[19] devised a new class of upconversion nanocrystals with a multilayer core–shell nanostructure by which the emission colour of the nanocrystals can be dynamically modulated by controlling the pulse duration of the excitation laser (Fig. 2j), suggesting their utility for full-colour volumetric 3D displays[19,99]. Table 1 provides an overview of the major advances and challenges in the field of upconversion nanocrystals.

Developing integrated strategies

To realize the myriad of opportunities for upconversion nanocrystals, readily scalable, hybrid materials need to be synthesized through an integrated approach whereby different structural constituents collectively contribute to the same challenge[2,3,20]. In this section, important recent advances in synthetic routes to mass production of multifunctional upconversion nanocrystals will be highlighted. The integration of upconversion nanocrystals with other functional materials by chemical approaches, including surface modification and functionalization, doping of semiconductor nanocrystals, core–shell processing and controlled nanocrystal assembly, is an indispensable element.

Surface modification and functionalization. Upconversion nanocrystals are usually synthesized by reacting lanthanide precursors in organic media in the presence of capping ligands for the benefit of size and shape uniformity. These nanocrystals are often heavily aggregated in aqueous solutions owing to the hydrophobic nature of the capping ligands, typically introduced during chemical synthesis to keep the crystals colloidally stable as they grow in organic media. To this end, surface modification techniques can be employed to render the nanocrystals hydrophilic and amenable for bioconjugation. Removal of the capping ligands, through either treatment with a strong acid[15] or an excess of ethanol[100], provides a direct solution for dispersion of the nanocrystals in aqueous media. Alternatively, post-treatment routes, based on layer-by-layer assembly[68], optimized silanization chemistry[101], ligand exchange[102] and polymer encapsulation[103,104], can lead to hydrophilic coatings at the crystal surface. In some special cases, where the capping ligands contain an alkene functional group with at least one hydrogen located at the double bond, it is possible to obtain water-soluble nanoparticles by means of direct conversion of the double bond into carboxylic acid with neutral or acidic permanganate[10,105].

Despite including a post-treatment for improved dissolution properties of upconversion nanocrystals, implementing the aforementioned approaches can be a tedious task because of the need for multistep processes involving product purification at various steps. In this regard, the synthesis of water-dispersible upconversion nanocrystals through one-pot processing is highly desirable. A particularly noteworthy aspect of this approach is the challenge of simultaneous control of crystallization and surface wetting characteristics. Recently, water-soluble $NaYF_4$:Yb,Er nanoparticles were successfully prepared by a facile one-pot hydrothermal synthesis[106]. A mixture of 11-aminoundecanoic acid and folic acid is the material of choice as surfactants to control the particle growth. This method simplifies the synthetic process relative to the multi-stage processing routes, but usually lacks precise control over the structure and morphology of the resultant nanomaterials.

Doping of semiconductor nanocrystals. Taking into account the fascinating physical properties of semiconductor nanocrystals, direct doping of lanthanides into the semiconductor nanocrystals is likely to impart additional functionalities and improved optical performance. For example, Er^{3+}-doped ZnO nanocrystals that exhibit visible emission under NIR light stimulation may find important applications in electroluminescent devices[36,107]. In another study, photovoltaic devices made of Ln^{3+}-doped TiO_2 nanomaterials showed a marked increase in energy conversion efficiency owing to enhancement of the NIR sunlight harvesting by lanthanide activators[74].

Gadolinium-based upconversion nanocrystals, such as $NaGdF_4$:Yb,Er, do possess magnetic properties, but they typically have much lower magnetization strength than conventional magnetic materials, such as iron oxide. An interesting task is to dope lanthanides directly into magnetic nanoparticles in an attempt to access dual upconversion and magnetic functions. For example, photoluminescence was observed in Tb^{3+}-doped γ-Fe_2O_3 nanoparticles[108]. In a recent twist[109], Yb^{3+},Er^{3+}-codoped SnO_2 nanomaterials showed paramagnetic behaviour, possibly arising from the strong exchange interaction between the unpaired electrons of lanthanides and the conduction electrons of n-type SnO_2.

Although photon upconversion is accessible in lanthanide-doped semiconductor nanocrystals, their luminescence intensities are much weaker than those obtained from fluoride nanocrystals of comparable size. The hardest part of investigations lies in the homogeneous incorporation of lanthanides into semiconductor host lattices. In most instances, lanthanides turned out to be bound to only the particle surfaces because of the charge mismatches and the large size discrepancy between the lanthanides and host cations[110].

Core–shell processing. The core–shell approach for assembling upconversion nanocrystals with other types of functional nanomaterials has proven effective in preparing multifunctional nanomaterials, such as magneto-upconversion supernanoparticles. Superparamagnetic Fe_3O_4 nanoparticles that can be magnetized strongly under the influence of an applied magnetic field have been suggested as prime candidates for magnetic resonance imaging (MRI) and X-ray CT applications[111,112] (Fig. 3a,b). The magnetic feature of upconversion nanocrystals can be introduced by direct coating with a thin layer of Fe_3O_4 materials[113]. However, the photon absorption by the Fe_3O_4 shell gives rise to slightly weakened emissions. This constraint may be partially satisfied by choosing Fe_3O_4 as the core together with a high-quality upconversion shell (Fig. 3c). In some cases, a thin layer of silica may be employed as an inner shell designed to mitigate the unwanted energy transfer from the upconversion nanocrystal to the magnetic core[114]. The trilayer core–shell strategy has proven effective, particularly when the size of the upconversion nanocrystal under study is much smaller than the magnetic core[115]. As the maximum imaging depth is limited by the allowed excitation and emission wavelengths of upconversion nanocrystals, it is obvious that the addition of magnetic components could constitute a combined platform for multi-modal imaging with maximum luminescence and penetration depth[103,116] (Fig. 3d–f).

The interaction between the core and shell components may offer a viable approach to tuning photon upconversion. This is exemplified by a recent work by Sharma *et al.*[117], who demonstrated electrically controllable fluorescence switching by coating SiO_2-modified $NaYF_4$:Yb,Er nanoparticles with a shell layer of redox-active sodium polyoxometalate. Similarly, a dual plasmon–upconversion function can be adopted by using noble metal-coupled upconversion

Table 1 | Advances and challenges in upconversion nanocrystals for various applications.

Application	Example	Size (nm)	Recent advances	Challenges	References
Bioimaging					
In vitro cell and tissue imaging	Y_2O_2S:Yb,Er(Tm) $NaYF_4$:Yb,Er(Tm)	200–400 18–30	Single-molecule imaging with sub-10 nm nanoparticles; highly specific staining and imaging of HeLa cells; *in vivo* NIR-to-NIR imaging; applicable for multimodal magnetic resonance imaging and X-ray computed tomography imaging	Imaging depths beyond 2 cm; mitigation of emission loss in ultrasmall nanoparticles; implementation of integrated confocal and high-resolution microscopy set-up; 3D image rendering capability	64,65,72,73,95
In vivo organism and animal imaging	Y_2O_3:Yb,Er $NaYF_4$:Yb,Er(Tm)	50–250 34			
Fluorescence diffuse optical tomography	$NaYF_4$:Yb,Tm	42			
Multimodal imaging	$NaGdF_4$:Yb,Er $NaLuF_4$:Yb,Tm	20–41 17			
Biodetection					
In vivo and *in vitro* detection of biomolecules	Y_2O_2S:Yb,Er(Tm) $Na(Y_{1.5}Na_{0.5})F_6$:Yb,Er $NaYF_4$:Yb,Er	480±30* 50 40	Single-particle sensitivity in complex media; ultralow limits of detection (1 ng μl^{-1} for DNA and 0.1 pg μl^{-1} for human chorionic gonadotropin); can be extended to multiplexed biosensing	Stabilization of nanoparticles in physiological buffers for long-term usage; facile control over particle bioconjugation; enhancement of sensing limit and precision	55,66–68
Cancer therapy					
Drug and gene delivery	$NaYF_4$:Yb,Er $NaYbF_4$:Er	30–100 21.7	Used for real-time monitoring and remote control of drug transport and release; can be used in multimodal photothermal and photodynamic therapy; capable of combining several imaging modalities	Precise control of target-specific drug release; assessment of tumour or tissue treatment at substantial depths; improvement of particle loading efficiency and biostability	69–71
Photodynamic and photothermal therapies	$NaYF_4$:Yb,Er $NaGdF_4$:Yb,Er	40–50 60			
Energy conversion					
Solar cells	$NaYF_4$:Yb,Er(Tm) $NaYF_4$:Yb,Er $NaYF_4$:Er†	16 400 70–80; 300–500	Successful demonstration of solar device integration with up- and down-converters; encouraging results on enhanced photovoltaic performance under simulated sunlight irradiation	Light harvesting in the NIR spectral range; pushing the limit for photon upconversion using sunlight irradiation; device configuration optimization for maximum energy conversion	16,18,86,87
Photocatalysis, water splitting, and so on	TiO_2:Er $NaYF_4$:Yb,Er	<15 20–50	Successful photocatalysis under NIR sunlight irradiation; photoelectrochemical water-splitting achievable with NIR laser irradiation	Rational structural design of integrated systems for enhanced photocatalytic performance	74–76
Displays					
RGB displays, 3D displays, and so on	$NaYF_4$:Yb,Er,Gd $NaYF_4$-based multishell particles‡	300 30–44	Tunable RGB and white-light output; volumetric full-colour display accessible; high spatial resolution and locally addressable colour gamut	Real-time, direct-view multicolour rendering; enhanced colour saturation and image display quality under low power laser manipulation; large-scale display capability with high spatial and temporal resolution	13,19,99
Others					
Security, barcoding, optical storage, upconversion lasers, RGB printing, thermal sensing, assembly, and so on	$NaYF_4$:Yb,Er(Tm) $NaYF_4$:Yb,Er(Tm) TbF_3	35–45 40 30	Rewritable optical storage; multicolour upconversion lasing capability; security printing with upconversion ink; multiplexed encoding addressability, and so on	Compact, portable read-out systems with large encoding capacity; cost-effective devices with fast response and high sensitivity	14,17,78–80,96

*Measured after silica coating. †Nanorods with a dimension of 70–80 nm in diameter and approximately 300–500 nm in length. ‡With a structural composition of $NaYF_4$:Nd,Yb@$NaYF_4$:Yb,Tm@$NaYF_4$@$NaYF_4$:Yb,Ho,Ce@$NaYF_4$. RGB, red–green–blue.

nanocrystals[49,118]. With their combination of different modalities, hybrid upconversion systems have potential in various applications, including solar-energy harvesting and conversion[119], photothermal therapy[120], X-ray CT and MRI (ref. 48), and biosensing[121].

Following core–shell processing, upconversion nanoparticles can be equipped with NIR-mediated photocatalytic capability on coating with a shell of TiO_2 or CdS material[122,123]. When $NaYF_4$:Yb,Er@TiO_2 core–shell nanoparticles are used as

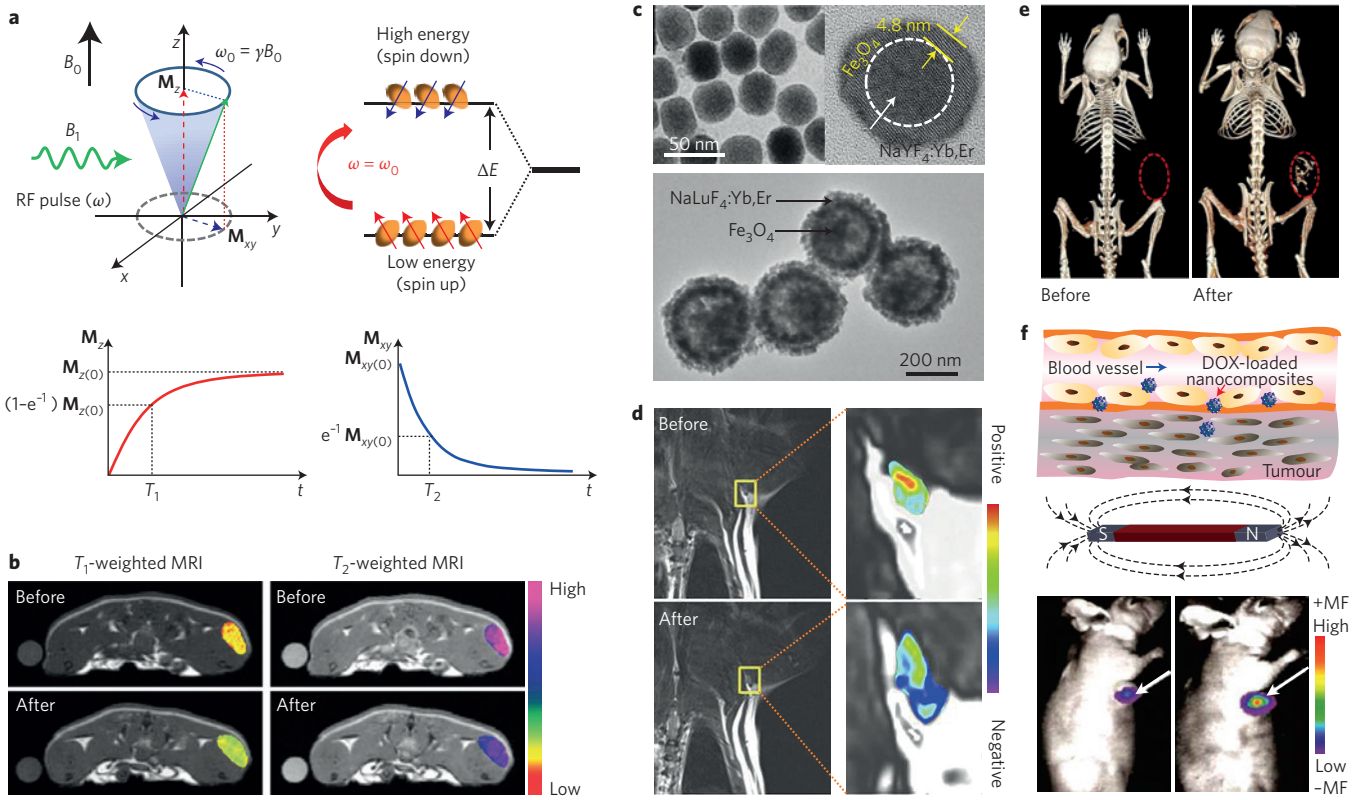

Figure 3 | Magnetism-coupling of upconversion nanocrystals through core–shell structuring for biomedical applications. a, Working principle of magnetic resonance imaging (MRI). The processing nuclei with the Larmor frequency of ω_0 ($\omega_0 = \gamma B_0$, where γ is the gyromagnetic ratio) at external constant magnetic field (B_0) can absorb the energy when the radiofrequency (RF) ω of the applied pulse $B_1(\omega)$ equals ω_0, resulting in an energy increase ΔE ($\Delta E = \hbar\omega_0$, where $\hbar$ is the reduced Planck constant). After switching off $B_1(\omega)$, the magnetization vector with longitudinal $\mathbf{M}_z$ and transverse $\mathbf{M}_{xy}$ components will return to its equilibrium state independently with characteristic T_1 and T_2 (spin-lattice and spin-spin relaxation times, respectively). **b**, *In vivo* T_1- and T_2-weighted magnetic resonance imaging using Fe_3O_4 nanoparticles. The colour scale represents image brightness. **c**, Transmission electron microscope images of $NaYF_4$:Yb,Er@Fe_3O_4 (top) and Fe_3O_4@$NaLuF_4$:Yb,Er (bottom) nanoparticles. **d**, *In vivo* magnetic resonance imaging of the armpit region of a mouse before and 10 min after the injection with $NaYF_4$:Yb,Tm@Fe_3O_4 nanoparticles (1.5 mg kg^{-1}), and the corresponding colour-mapped images. The colour scale shows the recorded intensity of the magnetic field. **e**, *In vivo* computed tomography volume-rendered imaging of the tumour-bearing mouse before and 30 min after intratumoral injection of Fe_3O_4@$NaLuF_4$:Yb,Er nanoparticles (1.5 mg kg^{-1}). The location of the tumour is marked by red circles. **f**, Schematic (top) and experimental results (bottom) of doxorubicin (DOX) drug delivery to tumour cells using DOX-modified Fe_3O_4@$NaYF_4$:Yb,Er nanoparticles. The experimental data suggest that an improved imaging resolution can be obtained with the magnetic field (MF; bottom right) compared with that without the magnetic field (bottom left). Figure reproduced with permission from: **b**, ref. 112, Wiley; **c** (top),**d**, ref. 113, Elsevier; **c** (bottom),**e**, ref. 116, Elsevier; **f** (bottom), ref. 114, American Chemical Society.

photoelectrodes in dye-sensitized solar cells with large bandgaps, the energy conversion efficiency of the photovoltaic devices can be considerably improved owing to the effective harvesting of sub-bandgap photons by the $NaYF_4$:Yb,Er component and its unique ability to convert the energy to ultraviolet–visible light for TiO_2 absorption[87,124].

A core–shell interfacial layer provides an important tool in tailoring composite functions, especially in situations where direct attachment of two disparate components is not an option. The most challenging technical assignment perhaps lies in the rational design and synthesis of the core–shell structure, while retaining the characteristic function of each building block. Some useful models have been developed, but the design of such systems is generally dominated by repeated trials of various reactions.

Controlled nanocrystal assembly. Co-assembling upconversion nanocrystals with other types of nanostructured building blocks offers the possibility of fabricating new classes of composite nanomaterials. When two functional components are comparable in size or difficult to combine via epitaxial growth, scalable assembly through direct conjugation has proven to be ideal for producing higher-order architectures with combined dual functionalities. For example, Fe_3O_4 nanoparticles pre-modified with dopamine can be immobilized onto poly(acrylic acid)-coupled $NaYF_4$:Yb,Er nanoparticles by a condensation reaction between the amino and carboxylic acid groups[120]. Building on the effect of crosslinking with 1,10-decanedicarboxylic acid (or 11-mercaptoundecanoic acid) molecules, a one-pot method was developed for the synthesis of Fe_3O_4-coupled $NaYF_4$:Yb,Er nanocrystals[125]. The patterning of magneto-upconversion superparticles could be readily achieved through magnetic manipulation[125].

Interestingly, oleic acid-capped $NaYF_4$:Yb,Er nanoparticles can be used as seeds to direct the growth of CdSe quantum dots from cadmium stearate and Bu_3PSe precursors in the presence of oleylamine (Fig. 4a(i))[126]. The positively charged amine ligand favours the growth of CdSe onto the $NaYF_4$:Yb,Er core. In this system, the red emission, as a result of energy transfer from upconverted Er^{3+} emission to CdSe, was observed under 980 nm excitation. This principle, which is illustrated in Fig. 4b, is applied to develop optoelectronic devices displaying sub-bandgap photoconductivity[126].

If the physical properties of building blocks are sensitive to the distance during the self-assembly process, silica can be employed

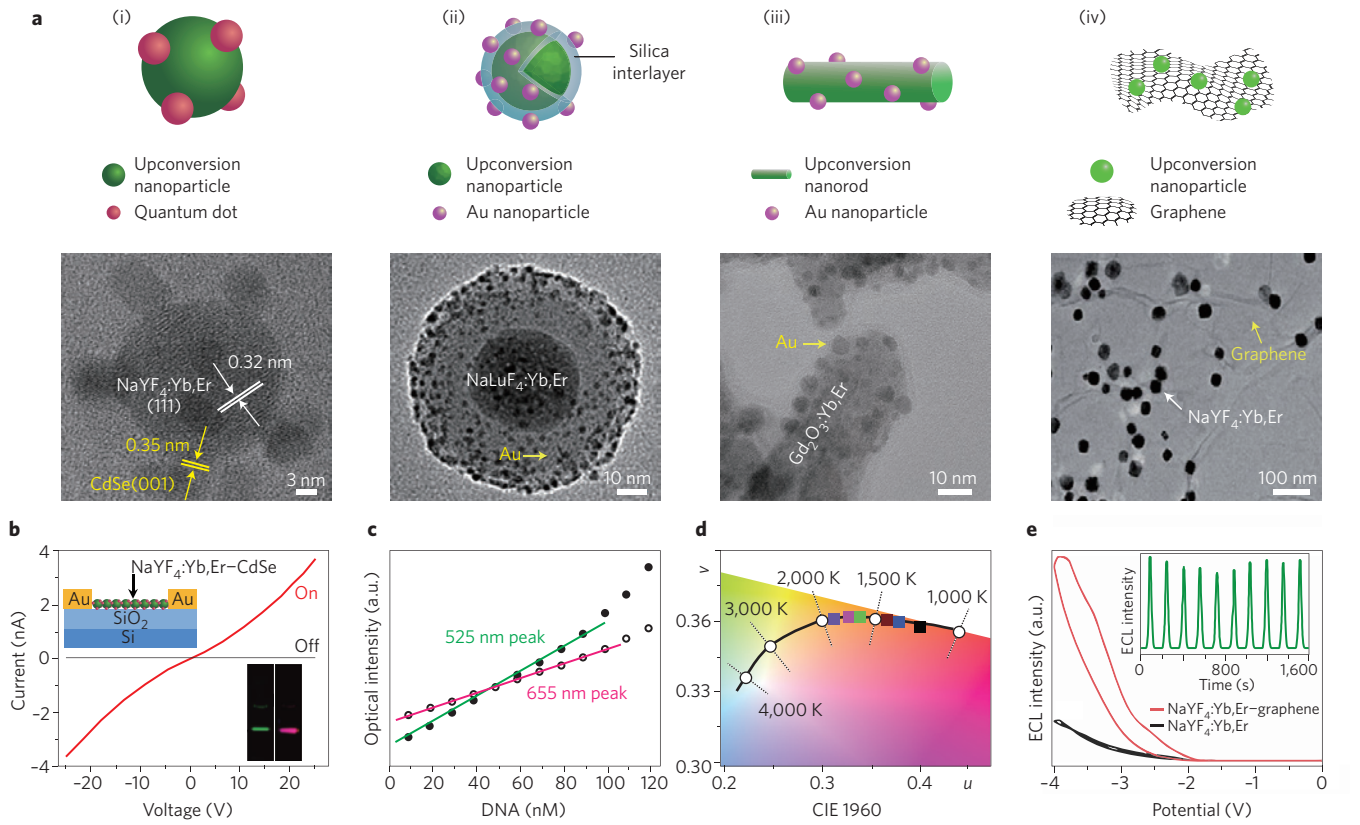

Figure 4 | Main strategies for multifunctionalization of upconversion nanocrystals for diverse applications. a, Top: Modification through use of quantum dots (i), gold nanoparticles (ii and iii) and graphene nanosheets (iv). Bottom: Corresponding transmission electron microscope images of the as-synthesized hybrid composite materials. **b**, Near-infrared light sensing by a phototransistor (top inset) made of $NaYF_4$:Yb,Er–CdSe hybrid nanoparticles. The bottom insets show the luminescent snapshots of colloidal $NaYF_4$:Yb,Er (left) and $NaYF_4$:Yb,Er–CdSe (right) nanoparticles under 980 nm excitation, indicating the occurrence of energy transfer between the $NaYF_4$:Yb,Er and CdSe nanoparticles. **c**, DNA concentration quantification (<100 nM) using Au nanoparticle-tethered $NaYF_4$:Yb,Er@SiO_2 hybrids. The measurement is enabled by harnessing the linear concentration dependence of the green (525 nm) and red (655 nm) emission of Er^{3+}. **d**, Temperature mapping (coloured squares) in the form of a CIE 1960 (u,v) chromaticity diagram, constructed by using Au particle-modified Gd_2O_3:Yb,Er nanorods. The matching of the emission location with the Planckian locus (curved line with circles) allows for temperature mapping in the range 300–2,000 K. **e**, Optoelectronic sensing built on the electrogenerated chemiluminescence (ECL) of graphene–$NaYF_4$:Yb,Er hybrid materials. The glassy carbon electrode made of graphene and upconversion nanocrystal composites offers enhanced ECL emission intensity (red line) compared with the electrode modified with solely $NaYF_4$:Yb,Er nanoparticles (black line). The inset indicates the emission stability of the hybrid material-modified electrode over repeated cycles (scan rate, 50 mV s^{-1}). Figure reproduced with permission from: **a** bottom (i), ref. 126, American Chemical Society; **a** bottom (ii), ref. 48, Elsevier; **a** bottom (iii), ref. 128, Wiley; **a** bottom (iv), ref. 131, Wiley; **b** bottom inset, ref. 126, American Chemical Society; **c**, ref. 127, American Chemical Society; **d**, ref. 128, Wiley; **e**, ref. 129, RSC.

as an interlayer to tune such distance, as shown in Fig. 4a(ii). This approach seems to work well for the plasmon–upconversion system[48]. DNA detection (down to 10 nM) was made possible by this approach, based on the linear dependence of emission intensity on DNA concentration (Fig. 4c)[127]. Gold nanoparticles can be directly attached onto upconversion nanorods (Fig. 4a(iii)), boosting the light excitation rate in the NIR regime for improved photovoltaic performance[86]. With a combination of Gd_2O_3:Yb,Er nanorods and Au nanoparticles, Debasu *et al.*[128] built an all-in-one optical heater-thermometer capable of temperature mapping within the range 300 to 2,000 K (Fig. 4d). The thermal-sensing principle was found to be associated with the cooperative effect of thermal equilibrium in the population of excited states on Er^{3+} upconversion.

Two-dimensional graphene sheets can also be used as scaffolds for the assembly of upconversion nanocrystals (Fig. 4a(iv)). A case in point is the preparation of graphene–$NaYF_4$:Yb,Er multifunctional materials by *in situ* growth of nanoparticles in the presence of graphene oxide[129]. The resulting hybrid materials can be further used to modify glassy carbon electrodes with dramatically enhanced electro-generated chemiluminescence (ECL) (Fig. 4e), offering them functionality for ECL-based sensing and optoelectronic applications[129]. Graphene oxide nanosheets decorated with upconversion nanocrystals exhibit a much improved nonlinear performance in the infrared regime[130,131]. Through surface modification of $NaYF_4$:Yb,Tm nanoparticles with MnO_2 nanosheets, a rapid, selective detection system for glutathione in aqueous solutions and living cells has been developed[132]. The detection was realized by monitoring the intensity level of upconversion luminescence, based on regulation of the glutathione–MnO_2 redox reaction.

Broader implications and outlook

Photon upconversion through the use of lanthanide-doped nanocrystals has been the focus of a growing body of research in recent years. Since the pioneering work in the early 2000s[35,38,133], upconversion nanocrystals have exhibited great potential for use in energy-related applications spanning from lighting to volumetric 3D displays to photovoltaics. In a parallel development, these nanomaterials have proven valuable as luminescent probes in the advancement of biological imaging with substantially improved spatial resolution. They can also be used to monitor levels of metal ions or biological species in the environment with high sensitivity.

A particularly noteworthy characteristic of upconversion nanocrystals is that they can be readily deposited as films from solution by various techniques. For microelectronic applications, the restructuring of the films is compatible with lithographic processes typically used in the semiconductor industry, because of the high photostability and thermal stability of the upconversion nanocrystals. In addition, these nanocrystals can be directly moulded with a soft, elastomeric stamp — a trait that makes them suitable for photonic integration on thin flexible substrates.

Despite the high stakes and great efforts undertaken in the research communities, there remain a number of constraints associated with upconversion nanocrystals at the most fundamental level. One of the restrictions is their low upconversion quantum efficiency. To date, the most efficient activators are limited to Er^{3+}, Tm^{3+} and Ho^{3+}, with a maximum internal quantum yield estimated to be 7.6% for $LiLuF_4$:Yb,Tm@$LiLuF_4$ nanoparticles under a light irradiance of 127 W cm^{-2} (ref. 134). Another challenge that the upconversion community faces is getting different wavelengths of light to interact with such optical nanomaterials. For the most part, one has to invent new particle systems with high absorbance at wavelengths that are not restricted to ~800, 980 or 1,500 nm. A set of specially crafted organic dyes provide interesting opportunities when bound to upconversion nanocrystals, because they permit a broadband excitation of the nanocrystals[16]. However, the mechanisms underlying the dye-sensitized upconversion process in these hybrid materials are so far not well understood.

Investigations of photon upconversion in lanthanide-doped nanocrystals have inspired many attempts to explore such a phenomenon occurring in carbon dots[135] or quantum dots[136]. Nonetheless, the risk of signal interference or misinterpreted data due to the diffraction of monochromator grating systems, for example, have to be cautiously considered[137].

Another area in need of improvement is the effective integration of commercially available imaging equipment with upconversion nanocrystals. Unlike fluorescent dyes and quantum dots, these nanocrystals require excitation in the infrared regime, which means that standard, commercial equipment cannot be used for quantitative measurements. Advances in fundamental nano-phenomena in upconversion require complex instrumentation, and a coordinated effort across a broad spectrum of disciplines will have a major impact in these areas.

For applications in biological systems, significant advances have occurred in the synthesis and multifunctionalization of upconversion nanocrystals with controlled size, shape and dissolution properties, but the ongoing work is less concerned with understanding of the complex processes, such as non-specific binding and loss of biological activities at the bio/nano interface, especially under physiological conditions. Standard protocols for robust particle coatings with active biomolecules remain vitally important, and innovation in bioconjugate techniques will certainly lead to enhanced long-term performance.

Recent studies addressed the important question of how upconversion nanocrystals impact living systems[138]. Though highly informative, the results that have confirmed low levels of cellular cytotoxicity in short-term assays may not be applicable to normal physiological conditions. Another area of concern is their adverse effects on the environment and human health. The experimental data collected thus far are clearly inadequate to determine whether the characteristics of upconversion nanocrystals lead to specific cytotoxic properties[139]. To reveal the particles' biodistribution, excretion pathways, metabolism, pharmacokinetics and pharmacodynamics in animal models, real-time, long-term tracking with custom-designed, built-in instruments is highly desired.

Received 30 April 2015; accepted 29 September 2015; published online 4 November 2015

References

1. Auzel, F. Upconversion and anti-Stokes processes with *f* and *d* ions in solids. *Chem. Rev.* **104,** 139–173 (2004).
2. Haase, M. & Schäfer, H. Upconverting nanoparticles. *Angew. Chem. Int. Ed.* **50,** 5808–5829 (2011).
3. Liu, X., Yan, C. & Capobianco, J. A. Photon upconversion nanomaterials. *Chem. Soc. Rev.* **44,** 1299–1301 (2015).
4. Bloembergen, N. Solid state infrared quantum counters. *Phys. Rev. Lett.* **2,** 84–85 (1959).
5. Ovsyakin, V. V. & Feofilov, P. P. Cooperative sensitization of luminescence in crystals activated with rare earth ions. *JETP Lett. Engl.* **4,** 317–318 (1966).
6. Esterowitz, L., Nooman, J. & Bahler, J. Enhancement in a Ho^{3+}–Yb^{3+} quantum counter by energy transfer. *Appl. Phys. Lett.* **10,** 126–127 (1967).
7. Johnson, L. F. & Guggenheim, H. J. Infrared-pumped visible laser. *Appl. Phys. Lett.* **19,** 44–47 (1971).
8. Bünzli, J. C. G. & Piguet, C. Taking advantage of luminescent lanthanide ions. *Chem. Soc. Rev.* **34,** 1048–1077 (2005).
9. Chen, G., Qiu, H., Prasad, P. N. & Chen, X. Upconversion nanoparticles: design, nanochemistry, and applications in theranostics. *Chem. Rev.* **114,** 5161–5214 (2014).
10. Yi, G. & Chow, G. Water-soluble $NaYF_4$:Yb,Er(Tm)/$NaYF_4$/polymer core/shell/shell nanoparticles with significant enhancement of upconversion fluorescence. *Chem. Mater.* **19,** 341–343 (2007).
11. Wang, F., Wang, J. & Liu, X. Direct evidence of a surface quenching effect on size-dependent luminescence of upconversion nanoparticles. *Angew. Chem. Int. Ed.* **49,** 7456–7460 (2010).
12. Höppe, H. A. Recent developments in the field of inorganic phosphors. *Angew. Chem. Int. Ed.* **48,** 3572–3582 (2009).
13. Sivakumar, S., van Veggel, F. C. J. M. & Raudsepp, M. Bright white light through up-conversion of a single NIR source from sol-gel-derived thin film made with Ln^{3+}-doped LaF_3 nanoparticles. *J. Am. Chem. Soc.* **127,** 12464–12465 (2005).
14. Zhang, C. *et al.* Luminescence modulation of ordered upconversion nanopatterns by a photochromic diarylethene: rewritable optical storage with nondestructive readout. *Adv. Mater.* **22,** 633–637 (2010).
15. Wang, F. *et al.* Tuning upconversion through energy migration in core–shell nanoparticles. *Nature Mater.* **10,** 968–973 (2011).
16. Zou, W., Visser, C., Maduro, J. A., Pshenichnikov, M. S. & Hummelen, J. C. Broadband dye-sensitized upconversion of near-infrared light. *Nature Photon.* **6,** 560–564 (2012).
17. Lu, Y. *et al.* Tunable lifetime multiplexing using luminescent nanocrystals. *Nature Photon.* **8,** 32–36 (2013).
18. Wang, J. *et al.* Photon energy upconversion through thermal radiation with the power efficiency reaching 16%. *Nature Commun.* **5,** 5669 (2014).
19. Deng, R. *et al.* Temporal full-colour tuning through non-steady-state upconversion. *Nature Nanotech.* **10,** 237–242 (2015).
20. Chan, E. M. Combinatorial approaches for developing upconverting nanomaterials: high-throughput screening, modeling, and applications. *Chem. Soc. Rev.* **44,** 1653–1679 (2015).
21. Liu, Y., Tu, D., Zhu, H. & Chen, X. Lanthanide-doped luminescent nanoprobes: controlled synthesis, optical spectroscopy, and bioapplications. *Chem. Soc. Rev.* **42,** 6924–6958 (2013).
22. Suyver, J. F. *et al.* Novel materials doped with trivalent lanthanides and transition metal ions showing near-infrared to visible photon upconversion. *Opt. Mater.* **27,** 1111–1130 (2005).
23. Dong, H., Sun, L.-D. & Yan, C.-H. Basic understanding of the lanthanide related upconversion emissions. *Nanoscale* **5,** 5703–5714 (2013).
24. Binnemans, K. Lanthanide-based luminescent hybrid materials. *Chem. Rev.* **109,** 4283–4374 (2009).
25. Dexter, D. L. A theory of sensitized luminescence in solids. *J. Chem. Phys.* **21,** 836–850 (1953).
26. Judd, B. R. Optical absorption intensities of rare-earth ions. *Phys. Rev.* **127,** 750–761 (1962).
27. Ofelt, G. S. Intensities of crystal spectra of rare-earth ions. *J. Chem. Phys.* **37,** 511–520 (1962).
28. Chan, E. M., Gargas, D. J., Schuck, P. J. & Milliron, D. J. Concentrating and recycling energy in lanthanide codopants for efficient and spectrally pure emission: the case of $NaYF_4$:Er^{3+}/Tm^{3+} upconverting nanocrystals. *J. Phys. Chem. B* **116,** 10561–10570 (2012).
29. Fischer, S., Steinkemper, H., Löper, P., Hermle, M. & Goldschmidt, J. C. Modeling upconversion of erbium doped microcrystals based on experimentally determined Einstein coefficients. *J. Appl. Phys.* **111,** 013109 (2012).
30. Dodson, C. M. & Zia, R. Magnetic dipole and electric quadrupole transitions in the trivalent lanthanide series: calculated emission rates and oscillator strengths. *Phys. Rev. B* **86,** 125102 (2012).
31. Wang, F. & Liu, X. Upconversion multicolor fine-tuning: visible to near-infrared emission from lanthanide-doped $NaYF_4$ nanoparticles. *J. Am. Chem. Soc.* **130,** 5642–5643 (2008).

32. Zhou, B., Tao, L., Tsang, Y. H. & Jin, W. Core–shell nanoarchitecture: a strategy to significantly enhance white-light upconversion of lanthanide-doped nanoparticles. *J. Mater. Chem. C* **1,** 4313–4318 (2013).
33. Mahalingam, V. *et al.* Bright white upconversion emission from $Tm^{3+}/Yb^{3+}/Er^{3+}$-doped $Lu_3Ga_5O_{12}$ nanocrystals. *J. Phys. Chem. C* **112,** 17745–17749 (2008).
34. Wang, H.-Q. & Nann, T. Monodisperse upconverting nanocrystals by microwave-assisted synthesis. *ACS Nano* **3,** 3804–3808 (2009).
35. Capobianco, J. A. *et al.* Optical spectroscopy of nanocrystalline cubic Y_2O_3:Er^{3+} obtained by combustion synthesis. *Phys. Chem. Chem. Phys.* **2,** 3203–3207 (2000).
36. Wang, X., Kong, X., Yu, Y., Sun, Y. & Zhang, H. Effect of annealing on upconversion luminescence of ZnO:Er^{3+} nanocrystals and high thermal sensitivity. *J. Phys. Chem. C* **111,** 15119–15124 (2007).
37. Dong, B. *et al.* Temperature sensing and *in vivo* imaging by molybdenum sensitized visible upconversion luminescence of rare-earth oxides. *Adv. Mater.* **24,** 1987–1993 (2012).
38. Stouwdam, J. W. & van Veggel, F. C. J. M. Near-infrared emission of redispersible Er^{3+}, Nd^{3+}, and Ho^{3+} doped LaF_3 nanoparticles. *Nano Lett.* **2,** 733–737 (2002).
39. Zhai, X. *et al.* Sub-10 nm $BaYF_5$:Yb^{3+},Er^{3+} core–shell nanoparticles with intense 1.53 μm fluorescence for polymer-based waveguide amplifiers. *J. Mater. Chem. C* **1,** 1525–1530 (2013).
40. Wang, J., Wang, F., Wang, C., Liu, Z. & Liu, X. Single-band upconversion emission in lanthanide-doped $KMnF_3$ nanocrystals. *Angew. Chem. Int. Ed.* **50,** 10369–10372 (2011).
41. Heer, S., Kömpe, K., Güdel, H. U. & Haase, M. Highly efficient multicolour upconversion emission in transparent colloids of lanthanide-doped $NaYF_4$ nanocrystals. *Adv. Mater.* **16,** 2102–2105 (2004).
42. Boyer, J.-C. & van Veggel, F. C. J. M. Absolute quantum yield measurements of colloidal $NaYF_4$:Er^{3+}, Yb^{3+} upconverting nanoparticles. *Nanoscale* **2,** 1417–1419 (2010).
43. Vetrone, F., Naccache, R., Mahalingam, V., Morgan, C. G. & Capobianco, J. A. The active-core/active-shell approach: a strategy to enhance the upconversion luminescence in lanthanide-doped nanoparticles. *Adv. Funct. Mater.* **19,** 2924–2929 (2009).
44. Zhang, F. *et al.* Direct imaging the upconversion nanocrystal core/shell structure at the subnanometer level: shell thickness dependence in upconverting optical properties. *Nano Lett.* **12,** 2852–2858 (2012).
45. Wang, Y.-F. *et al.* Rare-earth nanoparticles with enhanced upconversion emission and suppressed rare-earth-ion leakage. *Chem. Eur. J.* **18,** 5558–5564 (2012).
46. Dong, C. *et al.* Cation exchange: a facile method to make $NaYF_4$:Yb,Tm–$NaGdF_4$ core–shell nanoparticles with a thin, tunable, and uniform shell. *Chem. Mater.* **24,** 1297–1305 (2012).
47. Schietinger, S., Aichele, T., Wang, H.-Q., Nann, T. & Benson, O. Plasmon-enhanced upconversion in single $NaYF_4$:Yb^{3+}/Er^{3+} codoped nanocrystals. *Nano Lett.* **10,** 134–138 (2010).
48. Xing, H. *et al.* Multifunctional nanoprobes for upconversion fluorescence, MR and CT trimodal imaging. *Biomaterials* **33,** 1079–1089 (2012).
49. Sudheendra, L., Ortalan, V., Dey, S., Browning, N. D. & Kennedy, I. M. Plasmonic enhanced emissions from cubic $NaYF_4$:Yb:Er/Tm nanophosphors. *Chem. Mater.* **23,** 2987–2993 (2011).
50. Zhang, H. *et al.* Plasmonic modulation of the upconversion fluorescence in $NaYF_4$:Yb/Tm hexaplate nanocrystals using gold nanoparticles or nanoshells. *Angew. Chem. Int. Ed.* **122,** 2927–2930 (2010).
51. Saboktakin, M. *et al.* Metal-enhanced upconversion luminescence tunable through metal nanoparticle nanophosphor separation. *ACS Nano* **6,** 8758–8766 (2012).
52. Zhang, W., Ding, F. & Chou, S. Y. Large enhancement of upconversion luminescence of $NaYF_4$:Yb^{3+}/Er^{3+} nanocrystal by 3D plasmonic nano-antennas. *Adv. Mater.* **24,** OP236–OP241 (2012).
53. Huang, Q., Yu, J., Ma, E. & Lin, K. Synthesis and characterization of highly efficient near-infrared upconversion $Sc^{3+}/Er^{3+}/Yb^{3+}$ tridoped $NaYF_4$. *J. Phys. Chem. C* **114,** 4719–4724 (2010).
54. MacDougall, S. K. W., Ivaturi, A., Marques-Hueso, J., Krämer, K. W. & Richards, B. S. Ultra-high photoluminescent quantum yield of β-$NaYF_4$:10% Er^{3+} via broadband excitation of upconversion for photovoltaic devices. *Opt. Express* **20,** A879–A887 (2012).
55. Zhao, J. *et al.* Single-nanocrystal sensitivity achieved by enhanced upconversion luminescence. *Nature Nanotech.* **8,** 729–734 (2013).
56. Wang, J. *et al.* Enhancing multiphoton upconversion through energy clustering at sublattice level. *Nature Mater.* **13,** 157–162 (2013).
57. Zhang, J., Shade, C. M., Chengelis, D. A. & Petoud, S. A strategy to protect and sensitize near infrared luminescent Nd^{3+} and Yb^{3+}: organic tropolonate ligands for the sensitization of Ln^{3+} doped $NaYF_4$ nanocrystals. *J. Am. Chem. Soc.* **129,** 14834–14835 (2007).
58. Mauser, N. *et al.* Tip enhancement of upconversion photoluminescence from rare earth ion doped nanocrystals. *ACS Nano* **9,** 3617–3626 (2015).
59. Zhang, Y. & Liu, X. Shining a light on upconversion. *Nature Nanotech.* **8,** 702–703 (2013).
60. Zhou, B., Lin, H. & Pun, E. Y.-B. Tm^{3+}-doped tellurite glasses for fiber amplifiers in broadband optical communication at 1.20 μm wavelength region. *Opt. Express* **18,** 18805–18810 (2010).
61. Mai, H., Zhang, Y., Sun, L. & Yan, C. Highly efficient multicolor up-conversion emissions and their mechanisms of monodisperse $NaYF_4$:Yb,Er core and core/shell-structured nanocrystals. *J. Phys. Chem. C* **111,** 13721–13729 (2007).
62. Zhao, J. *et al.* Upconversion luminescence with tunable lifetime in $NaYF_4$:Yb,Er nanocrystals: role of nanocrystal size. *Nanoscale* **5,** 944–952 (2013).
63. Xie, X. *et al.* Mechanistic investigation of photon upconversion in Nd^{3+}-sensitized core–shell nanoparticles. *J. Am. Chem. Soc.* **135,** 12608–12611 (2013).
64. Zijlmans, H. J. *et al.* Detection of cell and tissue surface antigens using up-converting phosphors: a new reporter technology. *Anal. Biochem.* **267,** 30–36 (1999).
65. Nyk, M., Kumar, R., Ohulchanskyy, T. Y., Bergey, E. J. & Prasad, P. N. High contrast *in vitro* and *in vivo* photoluminescence bioimaging using near infrared to near infrared up-conversion in Tm^{3+} and Yb^{3+} doped fluoride nanophosphors. *Nano Lett.* **8,** 3834–3838 (2008).
66. Hampl, J. *et al.* Upconverting phosphor reporters in immunochromatographic assays. *Anal. Biochem.* **288,** 176–187 (2001).
67. van de Rijke, F. *et al.* Up-converting phosphor reporters for nucleic acid microarrays. *Nature Biotechnol.* **19,** 273–276 (2001).
68. Wang, L. *et al.* Fluorescence resonant energy transfer biosensor based on upconversion-luminescent nanoparticles. *Angew. Chem. Int. Ed.* **44,** 6054–6057 (2005).
69. Yang, Y., Velmurugan, B., Liu, X. & Xing, B. NIR photoresponsive crosslinked upconverting nanocarriers toward selective intracellular drug release. *Small* **9,** 2937–2944 (2013).
70. Wang, C., Cheng, L. & Liu, Z. Drug delivery with upconversion nanoparticles for multi-functional targeted cancer cell imaging and therapy. *Biomaterials* **32,** 1110–1120 (2011).
71. Idris, N. M. *et al. In vivo* photodynamic therapy using upconversion nanoparticles as remote-controlled nanotransducers. *Nature Med.* **18,** 1580–1585 (2012).
72. Wu, S. *et al.* Non-blinking and photostable upconverted luminescence from single lanthanide-doped nanocrystals. *Proc. Natl Acad. Sci. USA* **106,** 10917–10921 (2009).
73. Gargas, D. J. *et al.* Engineering bright sub-10-nm upconverting nanocrystals for single-molecule imaging. *Nature Nanotech.* **9,** 300–305 (2014).
74. Obregón, S., Kubacka, A., Fernández-García, M. & Colón, G. High-performance Er^{3+}–TiO_2 system: dual up-conversion and electronic role of the lanthanide. *J. Catal.* **299,** 298–306 (2013).
75. Qin, W., Zhang, D., Zhao, D., Wang, L. & Zheng, K. Near-infrared photocatalysis based on YF_3:Yb^{3+},Tm^{3+}/TiO_2 core/shell nanoparticles. *Chem. Commun.* **46,** 2304–2306 (2010).
76. Chen, C. K., Chen, H. M., Chen, C.-J. & Liu, R.-S. Plasmon-enhanced near-infrared-active materials in photoelectrochemical water splitting. *Chem. Commun.* **49,** 7917–7919 (2013).
77. Niu, W. *et al.* 3-Dimensional photonic crystal surface enhanced upconversion emission for improved near-infrared photoresponse. *Nanoscale* **6,** 817–824 (2013).
78. Zhu, H. *et al.* Amplified spontaneous emission and lasing from lanthanide-doped up-conversion nanoparticles. *ACS Nano* **7,** 11420–11426 (2013).
79. Wang, J. *et al.* Near-infrared-light-mediated imaging of latent fingerprints based on molecular recognition. *Angew. Chem. Int. Ed.* **53,** 1616–1620 (2014).
80. Meruga, J. M., Baride, A., Cross, W., Kellar, J. J. & May, P. S. Red-green-blue printing using luminescence-upconversion inks. *J. Mater. Chem. C* **2,** 2221–2227 (2014).
81. van der Ende, B. M., Aarts, L. & Meijerink, A. Near-infrared quantum cutting for photovoltaics. *Adv. Mater.* **21,** 3073–3077 (2009).
82. Jang, H. S., Woo, K. & Lim, K. Bright dual-mode green emission from selective set of dopant ions in β-$Na(Y,Gd)F_4$:Yb,Er/β-$NaGdF_4$:Ce,Tb core/shell nanocrystals. *Opt. Express* **20,** 17107–17118 (2012).
83. Huang, X., Han, S., Huang, W. & Liu, X. Enhancing solar cell efficiency: the search for luminescent materials as spectral converters. *Chem. Soc. Rev.* **42,** 173–201 (2013).
84. van der Ende, B. M., Aarts, L. & Meijerink, A. Lanthanide ions as spectral converters for solar cells. *Phys. Chem. Chem. Phys.* **11,** 11081–11095 (2009).
85. Richards, B. S. Enhancing the performance of silicon solar cells via the application of passive luminescence conversion layers. *Sol. Energ. Mater. Sol. Cells* **90,** 2329–2337 (2006).

86. Li, Z. Q. *et al.* Core/shell structured $NaYF_4$:Yb^{3+}/Er^{3+}/Gd^{3+} nanorods with Au nanoparticles or shells for flexible amorphous silicon solar cells. *Nanotechnology* **23,** 025402 (2012).
87. Liang, L. *et al.* Highly uniform, bifunctional core/double-shell-structured β-$NaYF_4$:Er^{3+},Yb^{3+}@SiO_2@TiO_2 hexagonal sub-microprisms for high-performance dye sensitized solar cells. *Adv. Mater.* **25,** 2174–2180 (2013).
88. Gorris, H. H. & Wolfbeis, O. S. Photon-upconverting nanoparticles for optical encoding and multiplexing of cells, biomolecules, and microspheres. *Angew. Chem. Int. Ed.* **52,** 3584–3600 (2013).
89. Tu, D. *et al.* Time-resolved FRET biosensor based on amine-functionalized lanthanide-doped $NaYF_4$ nanocrystals. *Angew. Chem. Int. Ed.* **50,** 6306–6310 (2011).
90. Lu, Y. *et al.* On-the-fly decoding luminescence lifetimes in the microsecond region for lanthanide-encoded suspension arrays. *Nature Commun.* **5,** 3741 (2014).
91. Savchuk, O. A. *et al.* Er:Yb:NaY_2F_5O up-converting nanoparticles for sub-tissue fluorescence lifetime thermal sensing. *Nanoscale* **6,** 9727–9733 (2014).
92. Renero-Lecuna, C. *et al.* Origin of the high upconversion green luminescence efficiency in β-$NaYF_4$:2%Er^{3+},20%Yb^{3+}. *Chem. Mater.* **23,** 3442–3448 (2011).
93. Liu, Y., Wang, D., Shi, J., Peng, Q. & Li, Y. Magnetic tuning of upconversion luminescence in lanthanide-doped bifunctional nanocrystals. *Angew. Chem. Int. Ed.* **52,** 4366–4369 (2013).
94. Yang, Y. *et al.* Hydrothermal synthesis of $NaLuF_4$:^{153}Sm,Yb,Tm nanoparticles and their application in dual-modality upconversion luminescence and SPECT bioimaging. *Biomaterials* **34,** 774–783 (2013).
95. Sun, Y., Peng, J., Feng, W. & Li, F. Upconversion nanophosphors $NaLuF_4$:Yb,Tm for lymphatic imaging *in vivo* by real-time upconversion luminescence imaging under ambient light and high-resolution X-ray CT. *Theranostics* **3,** 346–353 (2013).
96. Ye, X. *et al.* Competition of shape and interaction patchiness for self-assembling nanoplates. *Nature Chem.* **5,** 466–473 (2013).
97. Zhang, Y. *et al.* Multicolor barcoding in a single upconversion crystal. *J. Am. Chem. Soc.* **136,** 4893–4896 (2014).
98. Lee, J. *et al.* Universal process-inert encoding architecture for polymer microparticles. *Nature Mater.* **13,** 524–529 (2014).
99. Wang, F. *et al.* Simultaneous phase and size control of upconversion nanocrystals through lanthanide doping. *Nature* **463,** 1061–1065 (2010).
100. Kumar, R., Nyk, M., Ohulchanskyy, T. Y., Flask, C. A. & Prasad, P. N. Combined optical and MR bioimaging using rare earth ion doped $NaYF_4$ nanocrystals. *Adv. Funct. Mater.* **19,** 853–859 (2009).
101. Li, Z., Zhang, Y. & Jiang, S. Multicolor core/shell-structured upconversion fluorescent nanoparticles. *Adv. Mater.* **20,** 4765–4769 (2008).
102. Li, L., Wu, P., Hwang, K. & Lu, Y. An exceptionally simple strategy for DNA-functionalized up-conversion nanoparticles as biocompatible agents for nanoassembly, DNA delivery, and imaging. *J. Am. Chem. Soc.* **135,** 2411–2414 (2013).
103. Xu, H. *et al.* Polymer encapsulated upconversion nanoparticle/iron oxide nanocomposites for multimodal imaging and magnetic targeted drug delivery. *Biomaterials* **32,** 9364–9373 (2011).
104. Lu, G. *et al.* Imparting functionality to a metal–organic framework material by controlled nanoparticle encapsulation. *Nature Chem.* **4,** 310–316 (2012).
105. Chen, Z. *et al.* Versatile synthesis strategy for carboxylic acid-functionalized upconverting nanophosphors as biological labels. *J. Am. Chem. Soc.* **130,** 3023–3029 (2008).
106. Zhou, J., Yao, L., Li, C. & Li, F. A versatile fabrication of upconversion nanophosphors with functional-surface tunable ligands. *J. Mater. Chem.* **20,** 8078–8085 (2010).
107. Iwan, S. *et al.* Green electroluminescence from an n-ZnO:Er/p-Si heterostructured light-emitting diode. *Physica B* **407,** 2721–2724 (2012).
108. Zhang, Y., Das, G. K., Xu, R. & Tan, T. T. Y. Tb-doped iron oxide: bifunctional fluorescent and magnetic nanocrystals. *J. Mater. Chem.* **19,** 3696–3703 (2009).
109. Sharma, S., Shah, J., Kotnala, R. K. & Chawla, S. Red upconversion luminescence and paramagnetism in Er/Yb doped SnO_2. *Electron. Mater. Lett.* **9,** 615–620 (2013).
110. Bol, A. A., van Beek, R. & Meijerink, A. On the incorporation of trivalent rare earth ions in II–VI semiconductor nanocrystals. *Chem. Mater.* **14,** 1121–1126 (2002).
111. Na, H. B., Song, I. C. & Hyeon, T. Inorganic nanoparticles for MRI contrast agents. *Adv. Mater.* **21,** 2133–2148 (2009).
112. Zeng, J. *et al.* Anchoring group effects of surface ligand on magnetic properties of Fe_3O_4 nanoparticles: towards high performance MRI contrast agents. *Adv. Mater.* **26,** 2694–2698 (2014).
113. Xia, A. *et al.* Core–shell $NaYF_4$:Yb^{3+},Tm^{3+}@Fe_xO_y nanocrystals for dual-modality T_2-enhanced magnetic resonance and NIR-to-NIR upconversion luminescent imaging of small-animal lymphatic node. *Biomaterials* **32,** 7200–7208 (2011).
114. Zhang, F. *et al.* Mesoporous multifunctional upconversion luminescent and magnetic "nanorattle" materials for targeted chemotherapy. *Nano Lett.* **12,** 61–67 (2012).
115. Hu, D., Chen, M., Gao, Y., Li, F. & Wu, L. A facile method to synthesize superparamagnetic and up-conversion luminescent $NaYF_4$:Yb,Er/Tm@SiO_2@Fe_3O_4 nanocomposite particles and their bioapplication. *J. Mater. Chem.* **21,** 11276–11282 (2011).
116. Zhu, X. *et al.* Core–shell Fe_3O_4@$NaLuF_4$:Yb,Er/Tm nanostructure for MRI, CT and upconversion luminescence tri-modality imaging. *Biomaterials* **33,** 4618–4627 (2012).
117. Zhai, Y., Zhu, C., Ren, J., Wang, E. & Dong, S. Multifunctional polyoxometalates-modified upconversion nanoparticles: integration of electrochromic devices and antioxidants detection. *Chem. Commun.* **49,** 2400–2402 (2013).
118. Zhang, F. *et al.* Fabrication of Ag@SiO_2@Y_2O_3:Er nanostructures for bioimaging: tuning of the upconversion fluorescence with silver nanoparticles. *J. Am. Chem. Soc.* **132,** 2850–2851 (2010).
119. Atre, A. C., García-Etxarri, A., Alaeian, H. & Dionne, J. A. Toward high-efficiency solar upconversion with plasmonic nanostructures. *J. Opt.* **14,** 024008 (2012).
120. Cheng, L. *et al.* Facile preparation of multifunctional upconversion nanoprobes for multimodal imaging and dual-targeted photothermal therapy. *Angew. Chem. Int. Ed.* **50,** 7385–7390 (2011).
121. Peng, J. *et al.* High-efficiency *in vitro* and *in vivo* detection of Zn^{2+} by dye-assembled upconversion nanoparticles. *J. Am. Chem. Soc.* **137,** 2336–2342 (2015).
122. Tang, Y., Di, W., Zhai, X., Yang, R. & Qin, W. NIR-responsive photocatalytic activity and mechanism of $NaYF_4$:Yb,Tm@TiO_2 core–shell nanoparticles. *ACS Catal.* **3,** 405–412 (2013).
123. Li, C., Wang, F., Zhu, J. & Yu, J. C. $NaYF_4$:Yb,Tm/CdS composite as a novel near-infrared-driven photocatalyst. *Appl. Catal. B Environ.* **100,** 433–439 (2010).
124. Zhang, J. *et al.* An upconversion $NaYF_4$:Yb^{3+},Er^{3+}/TiO_2 core–shell nanoparticle photoelectrode for improved efficiencies of dye-sensitized solar cells. *J. Power Sources* **226,** 47–53 (2013).
125. Shen, J., Sun, L.-D., Zhang, Y.-W. & Yan, C.-H. Superparamagnetic and upconversion emitting Fe_3O_4/$NaYF_4$:Yb,Er hetero-nanoparticles via a crosslinker anchoring strategy. *Chem. Commun.* **46,** 5731–5733 (2010).
126. Yan, C. *et al.* Near-IR photoresponse in new up-converting CdSe/$NaYF_4$:Yb,Er nanoheterostructures. *J. Am. Chem. Soc.* **132,** 8868–8869 (2010).
127. Li, Z., Wang, L., Wang, Z., Liu, X. & Xiong, Y. Modification of $NaYF_4$:Yb,Er@SiO_2 nanoparticles with gold nanocrystals for tunable green-to-red upconversion emissions. *J. Phys. Chem. C* **115,** 3291–3296 (2011).
128. Debasu, M. L. *et al.* All-in-one optical heater-thermometer nanoplatform operative from 300 to 2000 K based on Er^{3+} emission and blackbody radiation. *Adv. Mater.* **25,** 4868–4874 (2013).
129. Yin, M., Wu, L., Li, Z., Ren, J. & Qu, X. Facile *in situ* fabrication of graphene-upconversion hybrid materials with amplified electrogenerated chemiluminescence. *Nanoscale* **4,** 400–404 (2012).
130. Tao, L. *et al.* Fabrication of covalently functionalized graphene oxide incorporated solid-state hybrid silica gel glasses and their improved nonlinear optical response. *J. Phys. Chem. C* **117,** 23108–23116 (2013).
131. He, T. *et al.* Mechanism studies on the superior optical limiting observed in graphene oxide covalently functionalized with upconversion $NaYF_4$:Yb^{3+}/Er^{3+} nanoparticles. *Small* **8,** 2163–2168 (2012).
132. Deng, R., Xie, X., Vendrell, M., Chang, Y.-T. & Liu, X. Intracellular glutathione detection using MnO_2-nanosheet-modified upconversion nanoparticles. *J. Am. Chem. Soc.* **133,** 20168–20171 (2011).
133. Heer, S., Lehmann, O., Haase, M. & Güdel, H.-U. Blue, green, and red upconversion emission from lanthanide-doped $LuPO_4$ and $YbPO_4$ nanocrystals in a transparent colloidal solution. *Angew. Chem. Int. Ed.* **42,** 3179–3182 (2003).
134. Huang, P. *et al.* Lanthanide-doped $LiLuF_4$ upconversion nanoprobes for the detection of disease biomarkers. *Angew. Chem. Int. Ed.* **53,** 1252–1257 (2014).
135. Li, H. *et al.* Water-soluble fluorescent carbon quantum dots and photocatalyst design. *Angew. Chem. Int. Ed.* **49,** 4430–4434 (2010).
136. Deutsch, Z., Neeman, L. & Oron, D. Luminescence upconversion in colloidal double quantum dots. *Nature Nanotech.* **8,** 649–653 (2013).
137. Gan, Z., Wu, X., Zhou, G., Shen, J. & Chu, P. K. Is there real upconversion photoluminescence from graphene quantum dots? *Adv. Opt. Mater.* **1,** 554–558 (2013).
138. Gnach, A., Lipinski, T., Bednarkiewicz, A., Rybka, J. & Capobianco, J. A. Upconverting nanoparticles: assessing the toxicity. *Chem. Soc. Rev.* **44,** 1561–1584 (2015).
139. Li, R. *et al.* Surface interactions with compartmentalized cellular phosphates explain rare earth oxide nanoparticle hazard and provide opportunities for safer design. *ACS Nano* **8,** 1771–1783 (2014).

140. Prorok, K. *et al.* The impact of shell host ($NaYF_4/CaF_2$) and shell deposition methods on the up-conversion enhancement in Tb^{3+},Yb^{3+} codoped colloidal α-$NaYF_4$ core–shell nanoparticles. *Nanoscale* **6,** 1855–1864 (2014).
141. Lahoz, F., Martín, I. R. & Alonso, D. Theoretical analysis of the photon avalanche dynamics in Ho^{3+}-Yb^{3+} codoped systems under near-infrared excitation. *Phys. Rev. B* **71,** 045115 (2005).

Acknowledgements

The authors would like to acknowledge support through the Agency for Science, Technology and Research (A*STAR) (grant nos 122-PSE-0014 and 1231AFG028), the National Research Foundation and the Economic Development Board (Singapore-Peking-Oxford Research Enterprise), the National Natural Science Foundation of China (grant no. R-2014-S-009) through the NUS Research Institute at Suzhou, and the Australian Research Council (Centre of Excellence for Nanoscale BioPhotonics, grant no. CE140100003, and Future Fellowship, grant no. FT 130100517).

Additional information

Reprints and permissions information is available online at www.nature.com/reprints. Correspondence and requests for materials should be addressed to X.L. or D.J.

Competing financial interests

The authors declare no competing financial interests.